Enceladus: A significant plasma source for Saturn's magnetosphere

D. H. Pontius, Jr.

Physics Department, Birmingham-Southern College, Birmingham, Alabama, USA

T. W. Hill

Physics and Astronomy Department, Rice University, Houston, Texas, USA

Abstract. The Cassini Plasma Spectrometer has reported dramatic perturbations of the magnetospheric plasma flow in a region extending at least 30 satellite radii away from Saturn's small but active icy satellite Enceladus. We interpret these observations here by means of a steady-state model of the electrodynamic coupling between Enceladus and Saturn. Neutral water molecules from Enceladus are ionized, predominantly by charge exchange with ambient ions, to produce a pickup current that accelerates them to the local plasma velocity. The consequent addition of angular momentum requires Birkeland (magnetic-field-aligned) currents that couple the newly injected plasma to distant parts of the flux tube and ultimately to Saturn's ionosphere. The rate of local ionization in our model varies with the inverse square of distance from the satellite and is scaled by a free parameter proportional to the ratio of the total mass-loading rate to Saturn's ionospheric Pedersen conductance. To explain the observed velocity perturbations we require a total mass-loading rate $\gtrsim$ 100 kg/s if the conductance is $\gtrsim$ 0.1 S as expected. If the mass-loading region is not strongly coupled to Saturn's ionosphere, then the appropriate conductance is the Alfvén "wing" conductance $\sim$ 2 S, requiring more than an order of magnitude more mass loading. In either case, Enceladus is clearly implicated as a significant, if not dominant, source of Saturn's magnetospheric plasma.

1. Introduction

On 14 July 2005 the Cassini spacecraft flew by Saturn's satellite Enceladus, approaching to within 175 km from the surface, less than one satellite radius (1 R_{En} = 250 km). During parts of this encounter, the Cassini Plasma Spectrometer (CAPS) was favorably oriented to study ions moving at or near the corotation direction, which allowed a determination of the bulk flow velocity of the plasma. Details of these data and their analysis are discussed by *Tokar et al.* [2006], who conclude that the plasma was significantly slowed and deflected at several tens of R_{En} from the surface.

The situation appears similar to what was observed at Jupiter when the Galileo spacecraft flew by Io, with some important differences. In that case, the flow was deflected several Io radii away, with severely stagnated flow reported in the satellite's wake near closest approach [*Frank et al.*, 1996]. *Hill and Pontius* [1998, henceforth HP98] interpreted these observations in terms of concentrated mass loading in Io's extended atmosphere. A combination of charge exchange and electron impact ionization converts neutral particles from Io into ions, and their addition to the plasma requires redistributing momentum to accommodate them.

This redistribution is accomplished by electric currents to distant regions. For such severely stagnated flow, there should be sufficient time for conditions in the equatorial regions to be communicated by Alfvén waves to Jupiter's atmosphere and back, thus establishing a persistent electromagnetic coupling between them. *Goldreich and Lynden-Bell* [1969] established that the strength of the interaction in this case depends on the ratio of Io's conductance to the Pedersen conductance of Jupiter's ionosphere, while *Goertz* [1980] showed that mass loading is equivalent to a Pedersen conductance. The resulting current is referred to as a pickup current.

The role of pickup currents in the Io torus and their coupling with Jupiter's ionosphere have long been identified as having important consequences for magnetospheric convection. *Pontius and Hill* [1982] showed that mass injection and associated pickup currents in the torus are responsible for its observed 3-5% lag behind corotation [*R. Brown*, 1983; *M. Brown*, 1994]. That model treated azimuthal averages of all quantities. In contrast, HP98 treated the immediate vicinity of Io where mass loading is highly concentrated. They assumed uniform plasma mass loading per unit magnetic flux at all points within 1.5 Io radii from the center of Io, with a negligible source farther out. Their results indicate that at least several hundred kilograms per second are injected near Io, a significant fraction of the source rate for the entire Io torus.

There are important differences between the situations at Io and Enceladus. Most notably, the flow deflection at Enceladus is significant at least as far away as 30 satellite radii, as compared to just a few satellite radii in the case of Io. Enceladus' radius is about 7 times smaller than Io's, so the regions over which the flow is perturbed are comparable in volume. However, for Enceladus the neutrals originate from a much smaller region within that volume and expand outward from the source Thus, the mass-loading rate is likely to vary strongly with radial distance from Enceladus simply because the neutral density does. Indeed, the observed neutral H_2O density [*Waite et al.*, 2006] is reasonably well fit by assuming a $1/r^2$ decrease with distance r, as uniform outflow with negligible gravitation would imply. Hence, the model that HP98 developed for Io, where mass loading changes discontinuously from some constant value to zero, cannot be applied without modification to Enceladus.

Copyright 2006 by the American Geophysical Union.
0148-0227/06/$9.00

Our model assumes that the pick-up ion gyroradius is small compared to the length scale of the electric-field variations. This is a good approximation at Io, where the gyroradius is ~ 0.005 times Io's radius for an S^+ ion picked up at the full corotation speed. It is also a good approximation at Enceladus, where an H_2O^+ ion picked up at the full corotation speed has a gyroradius ~ 0.06 times the radius of Enceladus. The approximation is actually better than indicated by this ratio, both because most ions are picked up at less than the full corotation speed and because the length scale of the electric-field variation is $\gg R_{En}$ (see below).

It is not immediately clear whether conditions are right for Enceladus to maintain a persistent electrodynamic connection with Saturn as Io arguably does with Jupiter. In a region with arbitrarily distant boundaries, it is more appropriate to treat the redistribution of momentum along the magnetic field by means of standing Alfvén waves, the Alfvén wing model [*Neubauer*, 1980]. What distinguishes these limits is the wave propagation time between the source region and the planet's ionosphere versus the time required to convect through the source region. Let us compare these. Near Enceladus' orbit Saturn's magnetic field strength is about 325 nT, while the Cassini Radio and Plasma Wave Science experiment indicates an electron number density $\sim 70/\mathrm{cm}^3$ [*Tokar et al.*, 2006]. Assuming an average ion mass of 17 amu gives an Alfvén speed ~ 200 km/s. The density is high only near the equator, beyond which it drops exponentially, and most of the Alfvén transit time occurs within the first Saturn radius ($1R_S$ = 60,300 km) of the equatorial plane. Hence the round-trip communication time should be of order 10 minutes. In contrast, the difference between corotation and Enceladus' Kepler speed is 26.4 km/s, at which speed the plasma would take about 20 seconds to cross Enceladus, or about one-thirtieth the Alfvén wave transit time. However, there are two important factors that influence this comparison and imply that a clear conclusion cannot be drawn. First, mass loading appears to be distributed over a region ~ 30 times larger than the satellite itself, which implies a correspondingly longer convection time. Second, the very process of mass loading shields the electric field and slows the plasma, thus extending the interaction period. Indeed, the results of the present paper indicate that the convection field is reduced to very low values near Enceladus. Together, these factors imply a much longer transit time.

The present model follows HP98 in adopting the approach of *Goldreich and Lynden-Bell* [1969]. That is, the role of the ionosphere in accelerating the newly added plasma is explicitly treated, and magnetic perturbations are neglected when mapping currents and fields between the ionosphere and equatorial magnetosphere. We do not explicitly model the intermediate stage of the coupling process wherein stresses are transmitted through the intervening plasma by Alfvén waves. In contrast to our approach, the Alfvén wing model treats the waves explicitly but neglects the role of the ionosphere and of variations of the Alfvén velocity in the magnetosphere. Fortunately, our mathematical model for the mass-loading region can be readily modified to accommodate the Alfvén-wing paradigm, as we describe in section 5 below.

We find that the CAPS observations require a total mass-loading rate in the vicinity of Enceladus (within a few R_{En}) of a few hundred kilograms per second. This makes Enceladus a significant, if not dominant, source of Saturn's magnetospheric plasma. For example, *Eviatar and Richardson* [1985] inferred a value ~ 100 kg/s for the total mass-loading rate in Saturn's magnetosphere on the basis of Voyager flow observations, and a value ~ 1000 kg/s would make Enceladus competitive with Io despite its much smaller size.

2. Model description – shielding the convection electric field

Consider a magnetic flux tube convecting past Enceladus. We assume that neutral molecules leave Enceladus with speeds no more than several times the Enceladus escape speed (0.21 km/s) [*Hansen et al.*, 2006; *Waite et al.*, 2006], compared with the plasma speed of about 26.4 km/s relative to Enceladus, the difference between corotation and the Kepler speed. Hence the neutrals are essentially at rest relative to Enceladus, and when ionized they add no momentum to the flowing plasma. In the absence of coupling to remote regions, the plasma would simply slow to conserve momentum. However, when mass is loaded into a localized portion of a magnetic flux tube, that initiates coupling by magnetic field-aligned currents to remote regions, where perpendicular electric fields are required to complete the circuit [*Drell et al.*, 1965; *Neubauer*, 1980]. This electric field is then mapped back along magnetic field lines, accelerating the newly added plasma and diverting the flow everywhere along those field lines.

Our procedure for modeling follows that of HP98, in that we adopt a spin-aligned dipole to represent Saturn's magnetic field $\mathbf{B}$ and assume the currents to be small enough that the perturbation magnetic field is negligible compared to the background field. The Cassini magnetometer showed a perturbation field magnitude $\sim$ few nT in the region of interest, compared to a background field ~ 325 nT [*Dougherty et al.*, 2006], thus justifying our assumption. We assume that the ion mass-loading rate per unit volume varies as $1/r^2$ with distance r from the center of Enceladus. It is important to note that this "mass-loading rate" is really a momentum-loading rate because the ionization of neutral H_2O molecules from Enceladus is probably dominated by charge exchange with ambient water-group ions [*Tokar et al.*, 2006]. This process replaces a fast ion with a slow one but does not affect the local ion mass density (if the two particles undergoing charge exchange have the same mass). However, it requires the same addition of ion momentum, and hence the same pickup current, as if the new ions were created by "new" (photo- or electron impact) ionization.

We assume that all quantities are steady in Enceladus' frame. The relevant physical quantity for our model is the total ion mass-loading rate within a given flux tube per unit magnetic flux, *i.e.*, the convective time derivative

$$\dot{\eta} = \mathbf{v} \cdot \nabla \eta \tag{1}$$

where

$$\eta = \int \frac{n_i m_i}{B}\, dz \tag{2}$$

is the plasma mass per unit magnetic flux for ions of number density n_i and mass m_i. (Equation (1) refers to the flux-tube mass content of newly injected ions that require acceleration to the local plasma velocity. Because charge exchange is a significant, and probably dominant, contributor to the ionization rate, it follows that the total change of η along a streamline is significantly less, and probably much less, than indicated by (1).) The pickup current density, likewise integrated across the equatorial plasma sheet, is

$$\mathbf{J}_\perp = \frac{\dot{\eta}}{B}\,\mathbf{E} = \tilde{\Sigma}\,\mathbf{E} \tag{3}$$

where $\tilde{\Sigma}$ is defined implicitly as the effective pickup conductivity [*Goertz*, 1980; *Hill et al.*, 1983].

HP98 treated this problem for Io assuming mass loading to be confined to the interior of a single circular disk with constant source rate inside and zero outside. Currents diverging at the edge of this disk in the magnetospheric equatorial plane are balanced by diverging Pedersen currents at

magnetic conjugate points in the ionosphere. In that situation, the perturbation electric field inside the disk ΔE_i is related to the background convection electric field E_o by

$$\left(6\,\Sigma_P + \tilde{\Sigma}\right)\Delta E_i = \tilde{\Sigma}\,E_o \tag{4}$$

The right side represents the strength of the pickup current driven by the background convection electric field. The left side shows that the perturbation field has two effects. The first is the ionospheric closure current, which depends on the height-integrated ionospheric Pedersen conductivity Σ_P of each hemisphere (assumed to be constant). The factor of 6 combines a factor of 2 representing Saturn's two hemispheres, a factor of 3/2 from dipole mapping, and a factor of 2 because the ionospheric closure current flows outside as well as inside the magnetic footprint of the disk. The second term on the left of (4) reflects the pickup current due to the perturbation field. Like the ionospheric current, this perturbation pickup current is proportional to $\Delta\mathbf{E} = \mathbf{E} - \mathbf{E}_o$ at each point, so these two currents act together to balance the pickup current driven by the background field. They differ in that no current flows outside the flux tube in the plasma sheet where $\tilde{\Sigma} = 0$.

This last point introduces an important modification required for the present work. If mass loading is not zero outside the boundary but merely reduced, then the perturbation electric field will drive pickup currents there as well. The divergence of those additional, exterior currents augments that of the interior currents, just as happens with ionospheric Pedersen currents. Hence, the current divergence produced by the perturbation field depends on the sum of pick-up conductances inside and outside the boundary. In contrast, the current driven by the background electric field diverges only because of the change in ion pickup rate, so its divergence depends on the difference in pick-up conductances. Repeating the derivation of (4) using this logic for a circular edge across which $\tilde{\Sigma}$ changes discontinuously from $\tilde{\Sigma}^{\rm int}$ on the inside to $\tilde{\Sigma}^{\rm ext}$ outside yields

$$\left(6\,\Sigma_P + \tilde{\Sigma}^{\rm int} + \tilde{\Sigma}^{\rm ext}\right)\Delta E_i = \left(\tilde{\Sigma}^{\rm int} - \tilde{\Sigma}^{\rm ext}\right)E_0 \tag{5}$$

Within the boundary, the electric field is in the same direction as $\mathbf{E}_o$ and has constant magnitude $E_o - \Delta E_i$

If we now place another circular region of enhanced mass loading inside and concentric with the first region, it will react to the uniform field there just as the original disk reacted to $\mathbf{E}_o$. Currents diverging at that new edge behave similarly and reduce the field interior to it. Equation (5) still applies by using the appropriate interior and exterior conductances for that edge and replacing E_o with the constant electric field applied by the surrounding disk. The result indicates how much that additional edge contributes to shielding the applied background field inside its perimeter.

We note an additional complication required for full internal consistency. The electric field produced by each edge exterior to itself also drives pickup currents, and these will diverge at any surrounding edge of larger radius where the pickup conductance changes. Although this can be incorporated in our model, the technical details are beyond the scope of the present paper and do not significantly affect our conclusions, mainly because the exterior field decreases in magnitude with the inverse square of distance. We have found that including those currents changes the interior, shielded electric field by less than 10%. We ignore this complication in the remainder of this paper.

This same logic applies for a series of nested circular edges, and by extension we can pass to the limit of a continuously varying mass-loading rate. To model a cylindrically symmetric mass-loading rate with a radial gradient, we nest a large number N of concentric disks of radii r_i, where mass loading changes at the boundary of each disk i, thus changing the pickup conductance by $\tilde{\Sigma}_i - \tilde{\Sigma}_{i-1}$. Mass loading thus drives pickup currents that diverge at each disk's edge. Edge i reduces the field within it by

$$\Delta E_i = \frac{\tilde{\Sigma}_i - \tilde{\Sigma}_{i-1}}{6\,\Sigma_P + \tilde{\Sigma}_i + \tilde{\Sigma}_{i-1}}\left(E_0 - \sum_{j=1}^{i-1}\Delta E_j\right) \tag{6}$$

The summation is for all disks of larger radii, proceeding to smaller radii as the index j advances to higher values. The term in parentheses is E_{i-1}, the magnitude of the uniform electric field that would exist interior to r_{i-1} if mass loading remained constant at all points closer to the origin. This result extends the notion of shielding as it was previously developed for Io [*Goertz*, 1980; *Hill et al.*, 1983]. It describes the gradual reduction of an externally applied electric field that occurs when mass loading increases continuously as a body is approached.

Each edge's contribution to the total electric field is proportional to the analytical solution for a single edge given in the appendix of HP98. The only changes are that the net interior field $E_i - E_o$ in equation (A3) of HP98 is replaced with equation (6) above, and the radius a at which the interior and exterior solutions are joined is replaced with r_i. The total electric field at any point is determined by combining the background corotation field with the individual perturbation fields produced by all the edges. Hence, by specifying the radial dependence of $\dot{\eta}$, or equivalently $\tilde{\Sigma}$, the electric field can be calculated at any position.

3. Radial variation of mass loading

As input to our model for the Enceladus encounter, we require a description of the radial dependence of the mass-loading rate. We first set the ion source rate equal to

$$\dot{n}_i = \frac{n_n}{\tau} \tag{7}$$

where n_n is the local neutral number density and τ is the lifetime against ionization. As noted above, charge exchange is the most likely ionization process, and (7) applies to the number density of new ions that require acceleration, not to the total ion number density, whose enhancement is certainly smaller and probably much smaller than indicated by (7). Because charge exchange is important, a fully consistent model would incorporate the dependence of τ on the plasma flow velocity. Such variation is beyond the scope of the present approach, and we will treat τ as a constant whose value is to be determined by comparison with data. This approximation (among others) precludes the possibility of precise agreement with observations. However, our goal is to obtain empirical constraints on the total plasma mass-loading rate contributed by Enceladus, and our model is well suited for this because it depends strongly on the global morphology of plasma injection.

Direct measurements of water vapor above 175 km altitude by the Cassini Ion and Neutral Mass Spectrometer (INMS) during the 14 July 2005 Enceladus encounter [*Waite et al.*, 2006] indicate that the neutral number density can be represented roughly by

$$n_n = n_E\left(\frac{R_{En}}{r}\right)^2 \tag{8}$$

where n_E = surface density, and r is the spherical distance from Enceladus' center. The INMS data suggest a value $n_E \sim 10^7/cm^3$, but a stellar occultation observation at about the same time by the Cassini UltraViolet Imaging

Spectrometer (UVIS), which probes much closer to the surface than INMS, suggests a value closer to $n_E \sim 10^9/cm^3$ [*Hansen et al.*, 2006]. Lacking more detailed information, we adopt the $1/r^2$ radial dependence (8) but leave the value of n_E as a free parameter within the constraints provided by existing observations.

Taking the time derivative of (2) and substituting (7) and (8) gives

$$\dot{\eta} = \frac{n_E\, m_i\, R_{En}^2}{B\,\tau} \int_{-\infty}^{\infty} \frac{dz}{\rho^2 + z^2} = \frac{\pi\, n_E\, m_i\, R_{En}}{B\,\tau} \left(\frac{R_{En}}{\rho}\right) \quad (9)$$

in cylindrical (ρ, ϕ, z) coordinates centered on Enceladus. The factor f arises from terminating the integration at Enceladus' surface and equals $(2/\pi)\arcsin(\rho/R_{En})$ for $\rho < R_{En}$ and unity elsewhere. We have found that this correction factor has negligible impact on our solutions compared to the variations among the cases presented below, so we set it equal to unity in the remainder of this paper. Integration in z is along the unperturbed background magnetic field, assumed to maintain a constant (southward) direction and a constant magnitude $B = 325$ nT throughout the region where mass loading is significant. The total mass-loading rate $\dot{M}$ is found by integrating (9) times B across the area perpendicular to $\mathbf{B}$. However, the result diverges if (9) applies indefinitely far from Enceladus, which would be unphysical in any case. For example, outside the Hill radius for Enceladus 3.5 R_{En} the influence of Saturn's gravity dominates. Neutral particles that were viewed as freely escaping when close to Enceladus are more appropriately treated as being on trapped orbits about Saturn when outside the Hill radius. Rather than attempting to explicitly treat this and many other complex factors influencing how mass loading varies at large distances, we introduce an exponential factor into (9) to reduce the neutral density away from Enceladus:

$$\dot{\eta} = \frac{\pi\, n_E\, m_i\, R_{En}}{B\,\tau} \left(\frac{R_{En}}{\rho}\right) \exp\left[-\frac{\rho}{\rho_o}\right] \quad (10)$$

The length scale ρ_o will be treated as a free parameter to be determined by comparison with data. An alternative would be to truncate the integration at some maximum distance, but that sharp discontinuity would produce an abrupt shear in the plasma velocity, contrary to CAPS observations.

Equation (10) prescribes a functional form with one free parameter ρ_o that is almost sufficient for calculating the electric field and the resulting plasma flow. What remains is uncertainty in its absolute magnitude because both n_E and τ are poorly constrained. Equation (6) shows that solutions for the perturbation electric field scale according to the ratio of the effective pickup conductance $\tilde{\Sigma} = \dot{\eta}/B$ to ionospheric conductance Σ_P. We specify $\tilde{\Sigma}$ at the reference distance $\rho_E = R_{En}$ and denote the ratio $\tilde{\Sigma}/6\Sigma_P$ at that point by α_E, so that

$$\dot{\eta} = 6\, B\, \alpha_E\, \Sigma_P \left(\frac{R_{En}}{\rho}\right) \exp\left[-\frac{(\rho - R_{En})}{\rho_o}\right] \quad (11)$$

Our ignorance of the values of the individual parameters n_E and τ is thus combined into a single parameter α_E that determines our ability to match the velocity perturbations reported by *Tokar et al.* [2006]. The total mass-loading rate is now

$$\dot{M} = B \int_0^{\infty} \dot{\eta}(\rho)\, 2\pi\, \rho\, d\rho = 12\pi\, B^2\, R_{En}^2\, \alpha_E\, \Sigma_P \left(\frac{\rho_o}{R_{En}}\right) \quad (12)$$

Inserting nominal values gives

$$\dot{M} = 0.027\, \alpha_E \left(\frac{\Sigma_P}{0.1S}\right) \left(\frac{\rho_o}{R_E}\right) \text{kg/s} \quad (13)$$

By comparing the observed flow deflections to model results based on α_E and ρ_o, we can determine $\dot{M}$, with the caveat that the result is proportional to the value assumed for Σ_P.

4. Observed flow compared with model results

The flow perturbations observed during the 14 July 2005 encounter are shown in Figure 1 in the rest frame of Enceladus [*Tokar et al.* 2006], while Figure 2 shows the flow speeds at each position. The Cassini spacecraft spanned a wide range of displacements (from negative to positive) along all three axes, so the observed variations cannot be attributed solely to any particular coordinate. Strong asymmetries of the ionization (charge-exchange) rate can be expected along the z axis because the Enceladus neutral H_2O source appears to be strongly concentrated near its south pole region [*Hansen et al.*, 2006; *Waite et al.*, 2006] and along the x and y axes because of the complex interplay between the neutral source and the corotating background plasma. However, the constancy of electric potential along magnetic field lines implies that flow perturbations have translational symmetry along $\mathbf{B}$ (and hence z) near the equatorial plane. Accordingly, Figure 1 shows all quantities projected into the equatorial plane despite the steep inclination of the spacecraft trajectory to that plane.

Data are only available at those positions where the instrument was favorably oriented relative to the flow. Because the data were obtained at different radial ranges on the inbound and outbound trajectory, it is not possible to assess the symmetry of the flow directly. However, even a cursory inspection of these figures reveals the impossibility of fitting the inbound and outbound data well with a single model where mass loading is symmetric about Enceladus and decreases monotonically with distance. The most distant inbound observations at $\rho \sim 16\, R_{En}$ indicate flow speeds near corotation, which suggests that the bulk of shielding occurs closer to Enceladus. In general, a shielded region will be surrounded by faster flow on the flanks where surrounding streamlines are compressed together. The available outbound data are all beyond $\rho = 25\, R_{En}$, so if the flow pattern were symmetric about $y = 0$, then flow speeds would be at or above corotation there. Contrary to this expectation, the measured flow is definitely slowed on the outbound portion, starting from $\sim$ 17 km/s at the closest point and increasing to just below corotation (25.5 km/s) at the most distant point (40 R_{En}).

It appears unavoidable that the physical source is not symmetric about Enceladus, and it seems likely that its centroid is displaced either toward Saturn or downstream, if not both. Our model can be generalized to incorporate such asymmetries as further information becomes available, either from further observations or from further modeling efforts. In the meantime, comparisons with our model are necessarily a compromise between fitting the inbound data versus fitting the outbound data. Given the simplifications of our theoretical model compared to the real situation (which is itself still largely unknown in detail), we do not expect a detailed match, and our results should be viewed as providing only an order-of-magnitude representation of the true situation. The sample streamlines shown in Figure 1 are calculated for $\alpha_E = 2000$ and $\rho_o = 3.0\, R_{En}$, which corresponds to a total mass loading rate of about 160 kg/s if Σ_P

Table 1. Data for the six model implementations described in the text and shown in the figures. The first three are optimized to fit the inbound data, while the last three are optimized for the outbound data. Pairs of α_E and ρ_o were varied until a reasonable match to the flow-speed data was obtained. The implied mass-loading rate was then calculated using equation (13) with the assumption $\Sigma_P = 0.1$ S, which provides an effective lower limit.

Case	α_E	ρ_o/R_{En}	$\dot{M}$ (kg/s)
A	16000	2.0	865
B	2000	3.0	160
C	250	5.0	34
D	6000	6.5	1050
E	1500	8.5	345
F	450	11.5	140

= 0.1 S. These model results are an improvement over those shown by Tokar et al., which used a simpler computational algorithm. The present solutions were calculated using 480 equally spaced edges with radii ranging from 0.25 to 60 R_{En}, by which distance shielding had become negligible.

Table 1 presents model results for six pairs of α_E and ρ_o. The first three (A-C) are selected to bracket the range of acceptable fits to the inbound flow speed, as seen in Figure 2a. Case B provides the best fit, while A and C illustrate clearly inferior fits on either side. As discussed above, the inbound data suggest that most of the shielding occurs within ~ 15 R_{En}. This conclusion is in accord with the modeled radial profiles of E_i shown in Figure 3a, calculated from equation (6), which indicate the degree to which the external electric field is shielded at each radius. Flow speed data on the outbound portion exhibit more irregularity than those on the inbound, but Figure 2b shows that acceptable fits can be obtained with parameter pairs D - F. For this second set of trials, the modeled shielding region extends much farther out, as seen in the radial profiles of E_i in Figure 3b. The best agreement with the outbound data is provided by case E, with D and F illustrating less satisfactory parameter pairs.

Our identification of the best-fit parameters is somewhat subjective. Indeed, trying to apply a precise, quantitative measure of quality of fit is not justified in light of the discordance between the inbound and outbound data. When parameter pairs were varied, fairly good model agreements could be obtained (considering inbound and outbound data separately) until the source rate differed from those in cases B and E by a factor of about two. Hence, the mass-loading rates in Table 1 are meaningful to no better than a factor of two. Because the rates calculated for cases B and E themselves differ by about that much, we conclude that the overall mass-loading rate is $\sim$ (250 kg/s) $\times$ (Σ_P/0.1 S), to within a factor of order two.

5. The Alfvén-wing alternative

If the pickup currents are assumed to close through Alfvén wings instead of Saturn's ionosphere, the flow pattern can be calculated similarly by combining nested layers of the solution for a circular boundary given by *Neubauer* [1980]. Equation (6) for the shielded electric field still applies, except that Σ_P is replaced by $2/3\,\Sigma_A$, where the Alfvén conductance is $\Sigma_A = 1/\mu_0 V_A \sim 2$S for low Alfvén mach numbers. At a given value of α_E, shielding is equally effective for coupling to either the ionosphere or an Alfvén wing, but the implied mass-loading rate is higher by a factor of 3/2 for the Alfvén wing.

The resulting streamlines are only slightly different, as shown in Figure 4. The calculated flow speeds for these two cases are almost identical on the inbound trajectory. This will tend to occur where shielding is strong, because in those regions most contributions to the perturbation electric field come from the solutions interior to that location, and those are the same (uniform) for both situations. In contrast, the outbound solutions differ somewhat from each other because those points are much farther out where there is little shielding and the external solutions dominate. However, the difference is very small.

We therefore conclude that these data can be equally well fit by either model. However, for an Alfvén speed $V_A = 200$ km/s, the Alfvén conductance is larger than the minimum Pedersen conductance by a factor ~ 20. Given the reasonable agreement between the observed flow and the model for cases B (inbound) or E (outbound), the Alfvén wing model would thus require a much larger mass-loading rate, several thousand kilograms per second, to produce a comparable amount of flow diversion. While this is possible in principle, it lies outside the present range of empirical estimates. However, it must be recognized that the conductivity of Saturn's ionosphere is not well constrained observationally. Scaling from the case of Jupiter [*Strobel and Atreya*, 1983] suggests a value $\sim$ 0.1 - 1 S. If we were to adopt the lower value, the measured flow deflections would imply a total mass-loading rate $\gtrsim$ 100 kg/s ($\gtrsim 4{\times}10^{27}$ H_2O/s) from (11), which can be taken as a lower limit. A larger conductivity, as indicated by aeronomy models [*Moore et al.*, 2004; L. E. Moore, private communication, 2006], would imply a correspondingly larger mass-loading rate. For comparison, *Hansen et al.* [2006] conclude, from their UVIS stellar occultation results, that the H_2O escape rate from Enceladus is in the range 150 - 350 kg/s. Modeling of the remotely observed OH cloud [*Jurac et al.*, 2002; *Richardson and Jurac*, 2004] requires an H_2O source rate $\sim$ 300 kg/s according to the most recent estimate [*Richardson and Jurac*, 2005].

6. Summary and conclusions

We have presented a simple model that predicts how the corotational plasma flow should be affected by an enhanced rate of plasma mass loading in the vicinity of Enceladus. The spatial distribution of the mass-loading rate must be specified independently. The key difference between the present model and the model we previously developed for Io [HP98] is that the rate of mass loading per unit magnetic flux is allowed here to vary continuously with distance from the satellite. The result is a flow pattern that varies smoothly, with no abrupt change at any demarcation between regions with significant and negligible mass loading.

The particular model we adopt for the mass-loading rate is a parsimonious choice that assumes variation as the inverse square of radial distance and is characterized in magnitude by the parameters α_E and ρ_o (equation (13) and Table 1). No single set of parameters can fit the inbound and outbound flow observations simultaneously, but parameter sets B (inbound) and E (outbound) give reasonable fits to the observed velocity perturbations [*Tokar et al.*, 2006; Figures 1 and 2 above] and imply a total mass-loading rate near Enceladus of at least $\sim$ 250 kg/s, given that Σ_P is expected to have a value of at least $\sim$ 0.1 S. Larger values of Σ_P are anticipated [*Moore et al.*, 2004; L. E. Moore, private communication, 2006], and the alternative quantity Σ_A appropriate to the Alfven-wing model is much larger ($\sim$ 2 S). Thus the observed velocity perturbations appear to require a localized mass-loading rate that is considerably in excess of 100 kg/s. This would imply that Enceladus, besides being the obvious source of the particulate E ring [*Hill*, 1984; *Spahn et al.*, 2006], is also an important if not dominant source of Saturn's magnetospheric plasma [*Young et al.*, 2005].

Acknowledgments. We thank A. J. Dessler, R. E. Johnson, L. E. Moore, R. L. Tokar, and V. M. Vasyliunas for useful discussions, the two referees for useful suggestions, and the entire CAPS

instrument team for providing the observations on which this paper is based. D. Pontius thanks the space physics group at Rice University for hospitality during his sabbatical visit there during which this work was initiated, and Birmingham-Southern College for supporting his sabbatical leave. This work was supported in part by NASA JPL contract 1243218 to Southwest Research Institute and NASA grant NAG5-13048 to Rice University.

References

Brown, R. A. (1983), Observed departure of the Io plasma torus from rigid corotation with Jupiter, *Astrophys. J.*, 268, L47.

Brown, M. E. (1994), Observation of mass loading in the Io plasma torus, *Geophys. Res. Lett.*, 10, 847.

Dougherty, M. K., K. K. Khurana, C. T. Russell, and F. N. Neubauer (2005), Cassini magnetometer observations from Enceladus, paper presented at Magnetospheres of the Outer Planets conference, Leicester, UK.

Frank, L. A., W. R. Paterson, K. L. Ackerson, V. M. Vasyliunas, F. V. Coroniti, and S. J. Bolton (1996), Plasma observations at Io with the Galileo spacecraft, *Science*, 274, 394.

Goertz, C. K. (1980), Io's interaction with the plasma torus, *J. Geophys. Res.*, 85, 2949.

Goldreich, P., and D. Lynden-Bell (1969), Io, a Jovian unipolar inductor, *Astrophys. J.*, 156, 59.

Hansen, C. J., et al. (2006), Cassini UltraViolet Imaging Spectrograph (UVIS) investigation of Enceladus' water vapor plume, *Science*, in press.

Hill, T. W. (1984), Saturn's E ring, *Adv. Space Res.*, 4, 149.

Hill, T. W., and D. H. Pontius, Jr. (1998), Plasma injection near Io, *J. Geophys. Res.*, 103, 19,879.

Hill, T. W., A. J. Dessler, and C. K. Goertz (1983), Jovian magnetospheric models, in *Physics of the Jovian Magnetosphere*, edited by A. J. Dessler, pp. 353-394, chap. 10, Cambridge Univ. Press, New York.

Jurac, S., M. A. McGrath, R. E. Johnson, J. D. Richardson, V. M. Vasyliunas, and A. Eviatar (2002), Saturn, search for a missing water source, *Geophys. Res. Lett.*, 29, 2172, doi, 10.1029/2002GL015855.

Moore, L. E., M. Mendillo, I. C. F. Mueller-Wodarg, and D. L. Murr (2004), Modeling of global variations and ring shadowing in Saturn's ionosphere, *Icarus*, 172, 503.

Neubauer, F. M. , Nonlinear standing AlfvÈn wave current system at Io, theory (1980), *J. Geophys. Res.*, 85, 1171.

Pontius, D. H., Jr., and T. W. Hill (1982), Departure from corotation of the Io plasma torus, local plasma production, *Geophys. Res. Lett.*, 9, 1321.

Richardson, J. D., and S. Jurac (2004), A self-consistent model of plasma and neutrals at Saturn: the ion tori, *Geophys. Res. Lett.*, 31, L24803, doi:10.1029/2004GL020959.

Richardson, J. D., and S. Jurac (2005), Sources of magnetospheric neutrals and plasma, paper presented at Magnetospheres of the Outer Planets conference, Leicester, UK.

Strobel, D. F., and S. K. Atreya (1983), Ionosphere, *Physics of the Jovian Magnetosphere*, edited by A. J. Dessler, pp. 51-67, chap. 2, Cambridge Univ. Press, New York.

Tokar, R. L., et al. (2006), The interaction of the atmosphere of Enceladus with Saturn's plasma, *Science*, in press.

Waite, J. H., Jr., et al. (2006), The atmospheric plume of Enceladus as observed by the Cassini Ion Neutral Mass Spectrometer, *Science*, in press.

Young D. T., et al. (2005), Composition and dynamics of plasma in Saturn's magnetosphere, *Science*, 307, 1262.

D. H. Pontius, Jr., Birmingham-Southern College, Box 549022, Birmingham, AL 35254. (dpontius@bsc.edu)

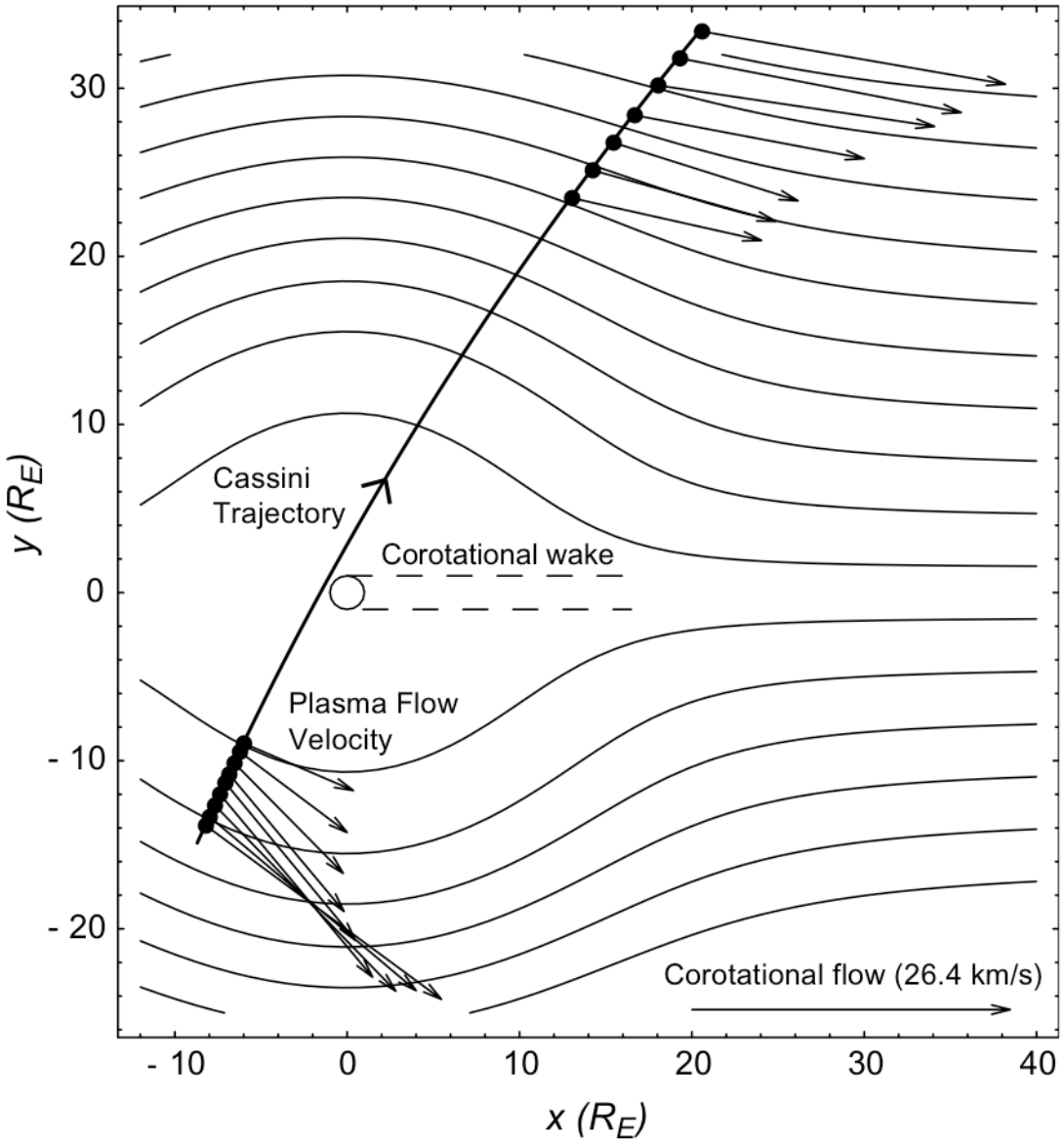

Figure 1. The arrows indicate the observed flow vectors reported by *Tokar et al.* [2006], shown with model streamlines calculated for case B (Table 1), corresponding to a mass-loading rate of 160 kg/s if $\Sigma_P = 0.1$ S. All quantities are projected into the equatorial plane. Coordinates x, y are centered on Enceladus, with x in the corotation direction and y toward Saturn. The z coordinate is out of the plane, and the abaxial coordinate ρ is the distance from the z axis.

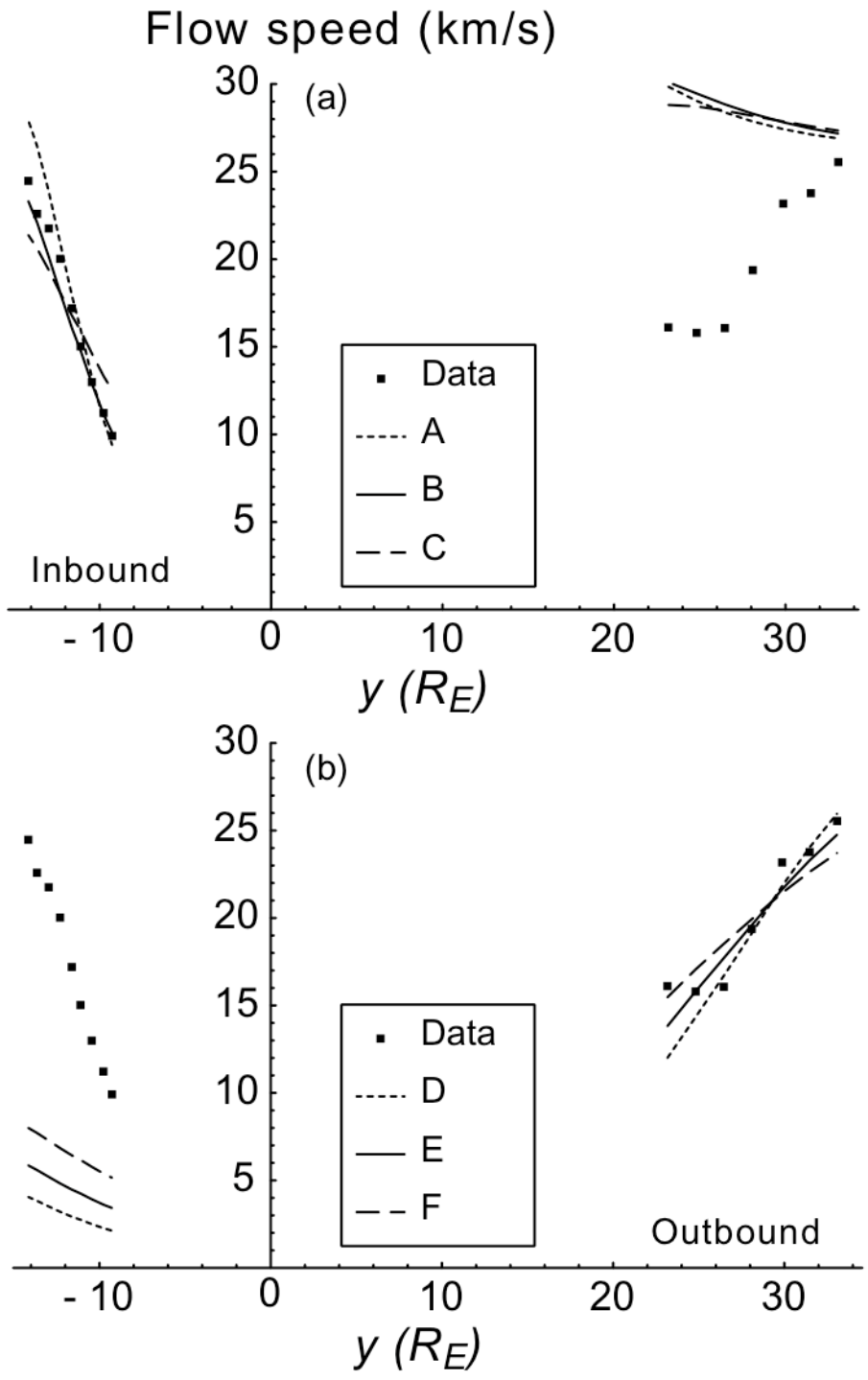

Figure 2. Flow speeds at Cassini's position as a function of the y coordinate (toward Saturn - see Figure 1). Dots are observed speeds associated with the vectors shown in Figure 1, and lines are model speeds corresponding to the parameter sets listed in Table 1. In (a, b), the parameter sets are chosen to produce optimal fits along the (inbound, outbound) portions of the trajectory, respectively.

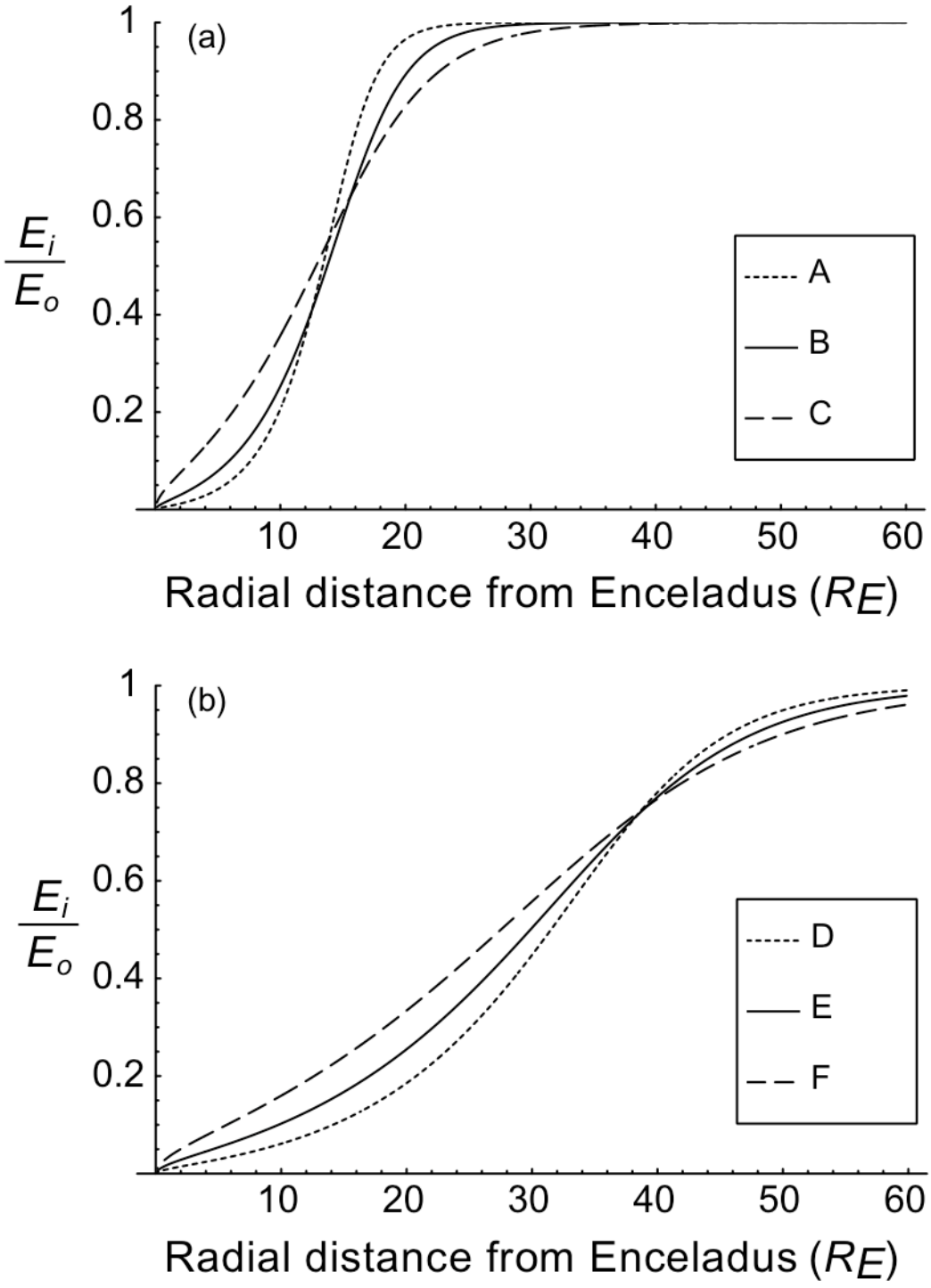

Figure 3. Variation of the shielded electric field with distance from Enceladus. At each distance, the various curves show the magnitudes of the uniform electric field that would exist inside that distance if mass loading were uniform between there and the origin. As in Figure 2, the parameter sets, listed in Table 1, are chosen for optimum fits to the (inbound/outbound) data in panels (a/b) respectively.

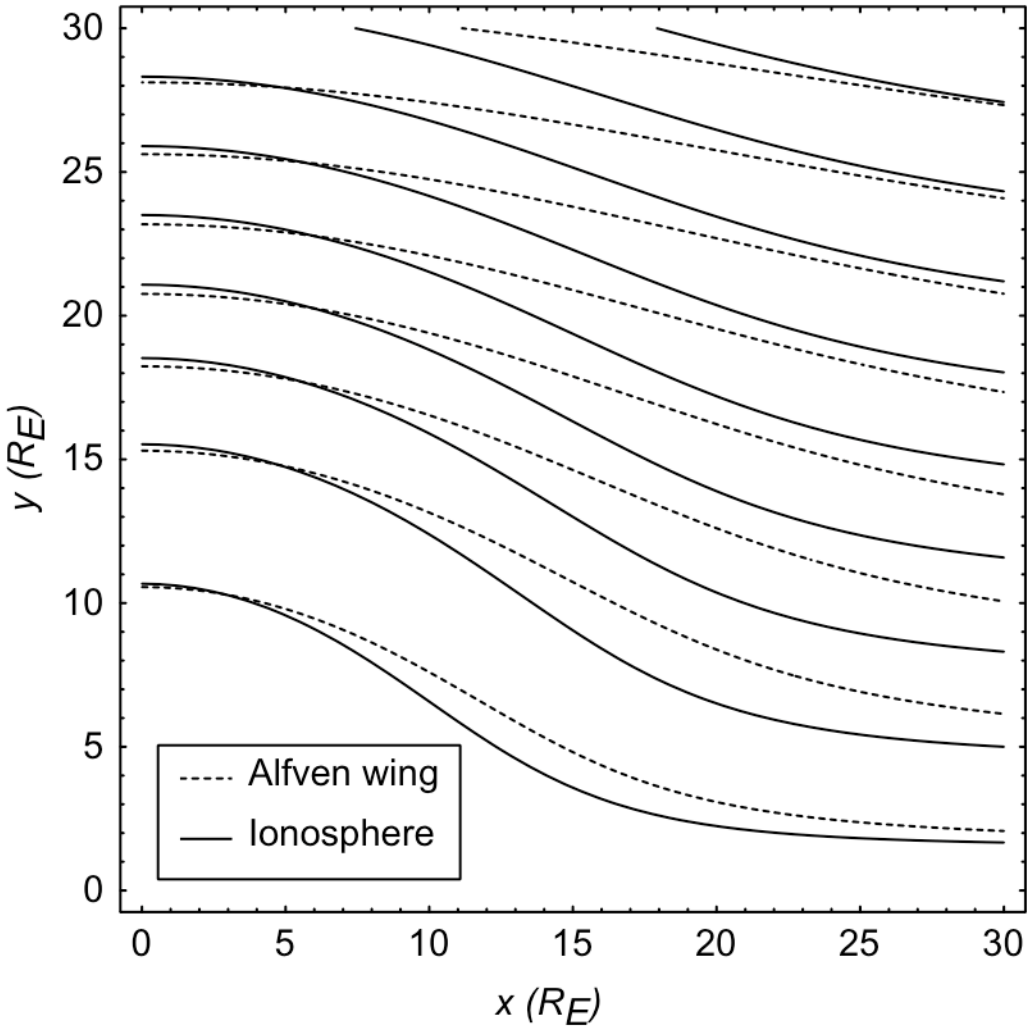

Figure 4. Streamlines for $\alpha_E = 2000$ and $\rho_o = 3.0\ R_{En}$ for coupling to Saturn's ionosphere (solid lines) and to Alfvèn wings (dashed).